Clin Orthop Relat Res (2014) 472:1106–1113
DOI 10.1007/s11999-013-3066-8

Clinical Orthopaedics and Related Research®
A Publication of The Association of Bone and Joint Surgeons®

SYMPOSIUM: THUMB CARPOMETACARPAL ARTHRITIS

In Vivo Pilot Study Evaluating the Thumb Carpometacarpal Joint During Circumduction

Akira Goto MD, Shuai Leng PhD, Kazuomi Sugamoto MD, William P. Cooney III MD, Sanjeev Kakar MD, Kristin Zhao PhD

Published online: 21 May 2013

Abstract

Background Analysis of arthrokinematics may have clinical use in the diagnosis of dynamic instability of the thumb and wrist. Recent technological advances allow noninvasive, high-resolution imaging of skeletal (thumb and carpal bones) structures during motion.

Questions/purposes The primary purpose of this study is to define the arthrokinematics, estimated joint contact patterns, and distribution ratios of the carpometacarpal joint of the thumb using four-dimensional CT (three-dimensional CT + time) and registration algorithms. The second purpose is to validate the accuracy of the approach.

Methods Four-dimensional CT scans were obtained using a nongated sequential scanning technique. Eighteen image volumes were reconstructed over a 2-second cycle during thumb circumduction in one healthy volunteer. Using a registration algorithm, serial thumb motions as well as estimated joint contact areas were quantified. To evaluate the accuracy of our approach, one cadaveric hand was used.

Results During circumduction, the ranges of motion of the thumb carpometacarpal joint were: flexion-extension, 27.3°; adduction-abduction, 66.9°; and pronation-supination, 10°. The magnitude of the translation of the center of the estimated joint contact area of the metacarpal was 4.1, 4.0, 1.0, and 1.5 mm when moving from the initial key pinch position to adduction, adduction to palmar abduction, palmar abduction to opposition, and opposition to the initial key pinch position, respectively. The maximum estimated contact area on the trapezium and on the metacarpal was in palmar abduction; the minimum was in adduction. Dominant central-volar contact patterns were observed on both the trapezium and the metacarpal bone except in adduction. This analysis approach had an average rotational error of less than 1°.

Each author certifies that he or she, or a member of his or her immediate family, has no funding or commercial associations (eg, consultancies, stock ownership, equity interest, patent/licensing arrangements, etc) that might pose a conflict of interest in connection with the submitted article.
All ICMJE Conflict of Interest Forms for authors and *Clinical Orthopaedics and Related Research* editors and board members are on file with the publication and can be viewed on request.
Clinical Orthopaedics and Related Research neither advocates nor endorses the use of any treatment, drug, or device. Readers are encouraged to always seek additional information, including FDA-approval status, of any drug or device prior to clinical use.
Each author certifies that his or her institution approved the human protocol for this investigation, that all investigations were conducted in conformity with ethical principles of research, and that informed consent for participation in the study was obtained.
This work was performed on-site at Mayo Clinic Rochester, Rochester, MN, USA.

A. Goto, K. Zhao (✉)
Biomechanics Laboratory, Division of Orthopedic Research, Mayo Clinic, Rochester, MN 55905, USA
e-mail: zhao.kristin@mayo.edu

S. Leng
Department of Radiology, Mayo Clinic, Rochester, MN, USA

K. Sugamoto
Department of Orthopedic Biomaterial Science, Osaka University, Osaka, Japan

W. P. Cooney III, S. Kakar
Department of Orthopedic Surgery, Mayo Clinic, Rochester, MN, USA

Conclusions During circumduction, the estimated joint contact area was concentrated on the central-volar regions of both the trapezium and the metacarpal bones except when the thumb was adducted.
Clinical Relevance This tool provides quantification of estimated joint contact areas throughout joint motion under physiological dynamic loading conditions; this tool may, in future studies, help to clarify some of the ways that joint mechanics might or might not predispose patients to arthritis.

Introduction

In vivo measurement of joint motion is important for understanding the effects of joint pathology (osteoarthritis or rheumatoid arthritis) or from injuries and to evaluate the outcome of clinical treatment. One of the purposes of a joint is to maintain an appropriate functional position throughout normal ROM. This ability is achieved by a complex balance between static and dynamic soft tissue stabilizers and bone contact or interaction. The relative stabilizing effect of these elements varies according to the joint position and motion. Subtle changes in in vivo measurement of joint motion may help clinicians predict instabilities related to abnormalities of these stabilizing mechanisms. This can be particularly useful in the diagnosis of joint dynamic instabilities, because conventional imaging often fails to diagnose these disorders.

Recent technological advances allow us to better visualize and characterize disease and injury of joints as well as to improve our understanding of the pathogenesis of progressive conditions. Four-dimensional CT (4-D; three-dimensional [3-D] CT + time) has high spatial and temporal resolution and provides us with dynamic image volumes during movement of the joint. In addition, robust registration techniques have been developed [8]. Using a combination of these techniques, we are able to evaluate the arthrokinematics at the joint. This technology enables us to visualize the arthrokinematics using the 3-D bone surface models generated from the sequential CT image volumes.

The primary purpose of this preliminary study was to define the arthrokinematics, estimated joint contact patterns, and distribution ratios within the normal thumb carpometacarpal (CMC) joint during circumduction in one healthy volunteer in vivo. The second purpose was to evaluate the accuracy of the approach, which used 4-D CT imaging and registration algorithms.

Materials and Methods

Four-dimensional CT Data Collection

One healthy 25-year-old volunteer without any hand or thumb pathology was recruited according to institutional review board guidelines. The volunteer reported no history of trauma or disease in the thumb and wrist joints. CT imaging was performed with a dual-source scanner (Siemens Definition FLASH; Siemens Healthcare, Forchheim, Germany) using a nongated sequential scanning technique [10]. The subject was positioned prone with the left forearm in neutral rotation and secured in a plastic cuff such that the wrist and base of the thumb were at the isocenter of the scanner. The initial step was to obtain a static scan of the thumb and hand using a standard CT imaging protocol: 120 kV, 250 mAs, 16 × 0.3 mm collimation, 1-second rotation, and a pitch of 0.8. In the second step, a 4-D CT scan was performed during circumduction motion of the left thumb, which was performed by having the volunteer move the thumb from the key pinch position into adduction (dorsal-radial extension), palmar abduction, and opposition (ulnovolar flexion) producing full circumduction before returning back to the original position. The motion was scanned continuously. The following imaging parameters were used during the 4-D CT scanning: 120 kV, 100 mAs/rotation, 0.28-second gantry rotation time, and 2 × 64 × 0.6 mm detector collimation (38.4 mm z-axis coverage). Eighteen image volumes were reconstructed over the 2-second trial using the commercially implemented dual-source cardiac reconstruction algorithm. DICOM images from the initial static scan and 4-D CT were saved to a personal computer for further analysis. The volume CT dose index (CTDIvol) of the 4-D CT scan was 70 mGy, which is equivalent to approximately two standard hand CT scans. This dose level is orders of magnitude lower than that which would generate any potential deterministic effect. Because there are no radiosensitive organs in the scan range, the stochastic effect is too low to be considered. The effective dose from a static CT scan is approximately 0.03 mSv [3]; therefore, the effective dose of the 4-D CT is approximately 0.06 mSv. This is a very low dose, only a small fraction of annual background radiation (average 3 mSv/year in the United States).

Image Segmentation

Analysis of the 4-D CT image volumes consists of segmentation (to delineate bone volumes) and voxel-based registration (to obtain bone kinematic information) [8]. Segmentation is the partitioning of digital image data into different regions based on the anatomy of interest. The goal of segmentation is to distinguish the objects (bone and soft tissue) from the background. Image segmentation is typically the initial step in object recognition, registration, and/or creating 3-D models of anatomical structures. In this study, we applied a 3-D region-growing method for segmenting the carpal bones [1, 12]. The process of 3-D

region-growing extracts a connected region of interest (ROI) by merging all voxels satisfying an aggregation criterion. In this method, a seed point inside the ROI is required to initialize the process. Starting from a manually located seed (a voxel contained within the bone of interest), adjacent regions that have similar densities as the seed point are merged. This process is continued until all voxels in the ROIs are assigned to their respective regions using a criterion that captures sharpness of region boundaries.

Registration

To achieve subvoxel accuracy, the CT images were interpolated before registration [7]. Voxel-based registration is a method for superimposing images based on similarity between two different images using the gray-value information in the CT images, which involves calculating the registration transformation by optimizing some measure calculated directly from the voxel values in the ROIs. The normalized correlation coefficient (NCC) was used as a measure of similarity in this approach. Using this method, the segmented bone data from the initial position were superimposed on the same bones in the images from two or more serially acquired thumb volumes [8]. This process continued until the NCC was maximized. The resulting transformation matrices were recorded, which resulted from the precise alignment of sequential image volumes during thumb motion. Imaging analysis was performed using Virtual Place-M software (Osaka University, Osaka, Japan).

Definition of the Anatomical Coordinate Systems for the Carpometacarpal Joint

To evaluate the thumb CMC joint motion using Euler angles, the anatomical coordinate system of the trapezium in the initial key pinch position was defined according to Cooney et al. (Fig. 1) [5]. Euler angles are a way to represent the orientation of an object in 3-D space using three sequential rotations. The anatomical coordinate system for the trapezium was defined as having its origin at the trapezium, scaphoid, and trapezoid junction center. The axes were associated with the functional axes of the thumb. The first rotation of the metacarpal in relation to the trapezium was flexion/extension about the Z axis, the second rotation was adduction/abduction about the X axis, and the last rotation was pronation/supination about the Y axis, as described by Wu et al. [15]. The movements of the first metacarpal relative to the trapezium were analyzed using the anatomical coordinate system of the thumb CMC joint. Resultant matrices were transformed to represent those of a right thumb and then the transformation matrices of the metacarpal relative to the trapezium were used to determine Euler angles as described previously. For this study, the initial key pinch position and three positions of the

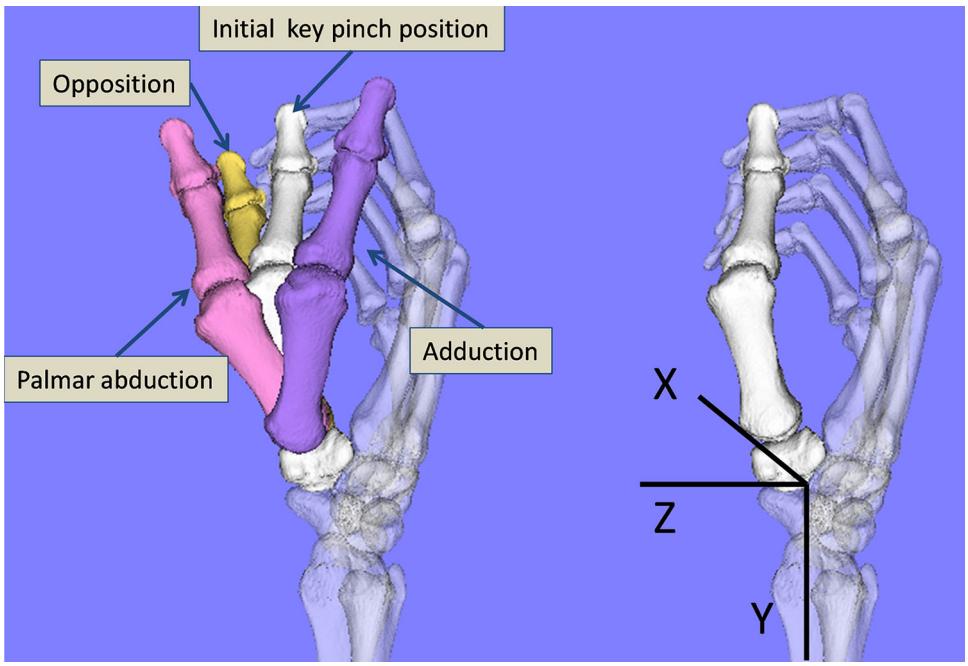

Fig. 1 Definition of the anatomical coordinate systems for the thumb CMC joint and description of the thumb positions during the circumduction movement. The anatomical coordinate systems are represented on the 3-D bone model of the trapezium according to Cooney et al. [5].

thumb in full circumduction were analyzed: adduction (dorsal radial extension), palmar abduction, and opposition (ulnovolar flexion).

Joint Proximities

In this study, the articular cartilage is assumed to be of uniform thickness; therefore, joint proximity serves as a surrogate for joint contact area. To calculate estimated joint contact areas, 3-D bone surface models were reconstructed from the segmented CT data using a marching cubes algorithm [11]. Bone surface models were constructed as continuous polygonal meshes and represented as a collection of 3-D points. Also, by classifying each vertex, the algorithm was able to generate more accurate surface models than schema based on edge detection or global thresholding, because the surface intersection points were interpolated on the lattice rather than being restricted to the lattice points themselves.

Using the kinematic data obtained from the image registrations, the bone surface models of the trapezium and metacarpal bones were precisely positioned to reproduce the bone orientations during each volume of the 4-D sequence. The reconstruction and visualization of the bone models were performed using custom software based on the Visualization Toolkit (Kitware, Clifton Park, NY, USA). The proximities at each position of the joint were then calculated (within prescribed thresholds: 1 mm, 2 mm, and 3 mm) and represented on the meshes of the subchondral bones with a prescribed threshold, presumably reflecting their joint contact areas. Euclidean distances between all points on the trapezium to all points on the metacarpal joint surface were obtained and displayed using a user-defined color scale (Fig. 2).

In addition to this calculation, estimated joint contact area distribution ratios were evaluated; these ratios quantify the frequency of contact within nine anatomical regions on each bone during the circumduction movement [2]. The distribution ratios in each region were expressed as percentages (Fig. 3). Furthermore, we displayed the movements of the centroids of the estimated joint contact areas (within the 1mm threshold) and quantified the maximum distance among the centroids during the thumb circumduction movement (Fig. 4).

Accuracy of the Four-dimensional CT Approach

A fresh-frozen cadaveric forearm amputated just distal to the elbow was used for the study. The hand, radius, and ulna bones were firmly mounted onto a custom-made motion simulator. The thumb was mounted onto an acrylic paddle. Two linear slides under the paddle allowed it to have composite motions. A programmable Si5580 step motor and driver (Applied Motion Products, Watsonville, CA, USA) produced belt-driven motion of the paddle allowing the thumb to perform periodic (repeatable from cycle to

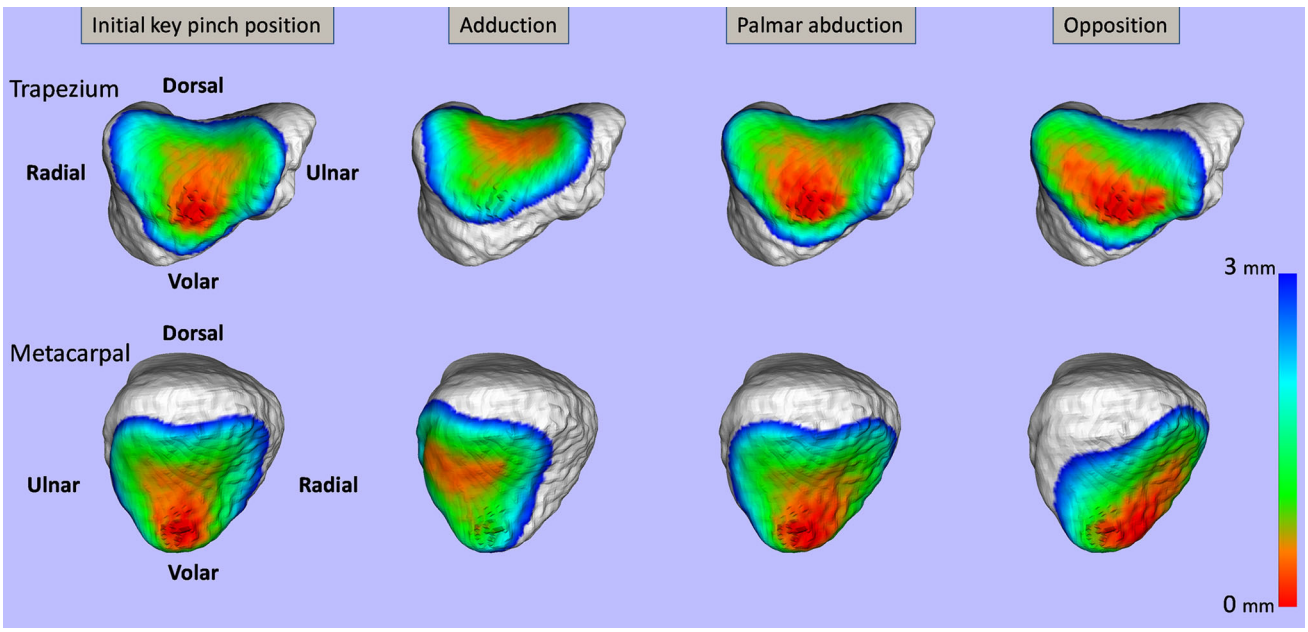

Fig. 2 The estimated joint contact areas of the trapezium and metacarpal bones in each thumb position. The joint proximities obtained as Euclidean distance measures were displayed using a color scale. The red areas indicate the closest point in each thumb position. Except for the adduction position, dominant central-volar contact patterns were seen on both the trapezium and metacarpal bones. Also, the estimated joint contact area in the opposition position was along the radiovolar perimeter of the thumb CMC joint.

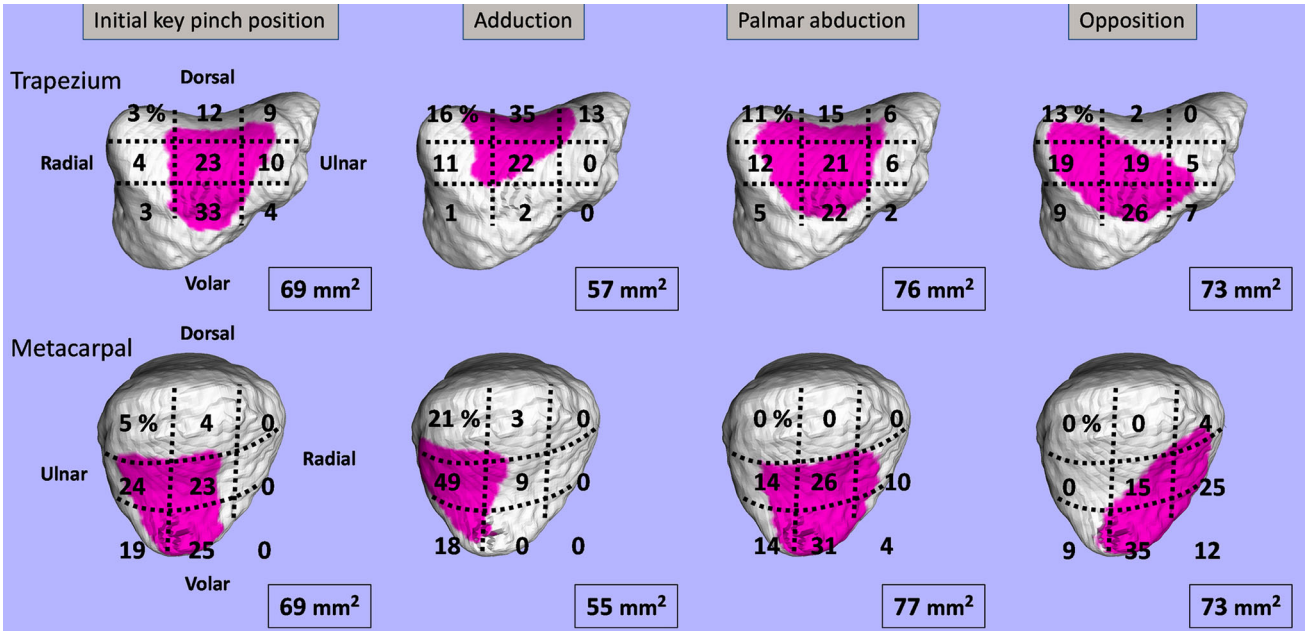

Fig. 3 The distribution ratios of the estimated joint contact areas in each anatomic region for each position. The minimum contact area on the trapezium was 57 mm^2, which was located on the dorsal-central side of the articular surface with the thumb in the adduction position. The maximum contact area was 76 mm^2 on the radiocentral part with the thumb in palmar abduction. In the opposition position, linear contact was seen on the radiovolar portion of the articular surface; the estimated joint contact area was 73 mm^2. The minimum contact area on the metacarpal bone was 55 mm^2 and was located in the midportion of the radial side of the articular surface in the palmar abduction position. The maximum contact area was 77 mm^2 and was located on the center of the articular surface.

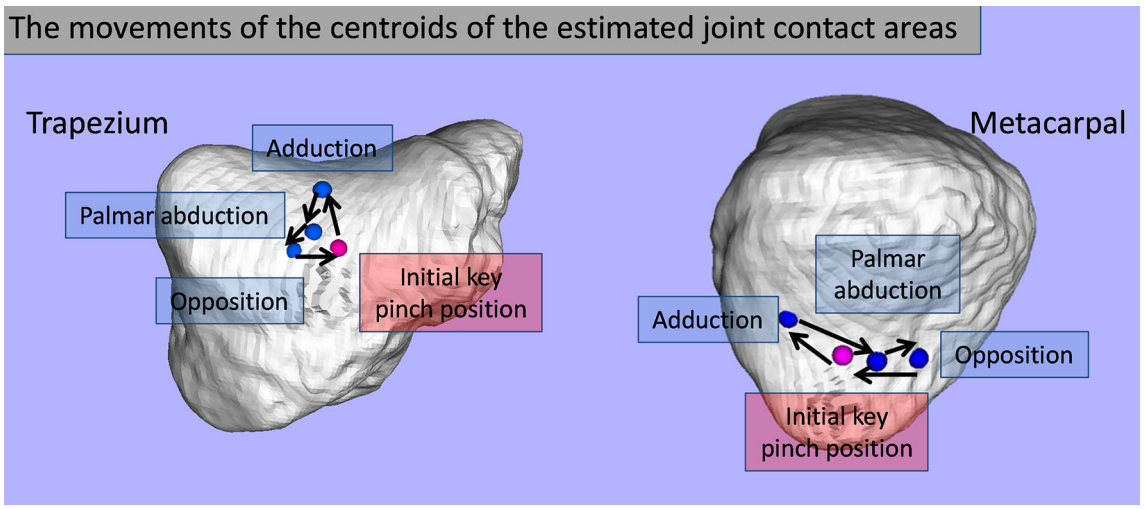

Fig. 4 The trajectories of the centroids of the estimated joint contact areas. The centroids on the trapezium were located in the central region of the articular surface. The centroid on the trapezium showed the movement in the volar and dorsal direction during thumb circumduction motion. Meanwhile, the centroid on the metacarpal bone moved in a radial and ulnar direction. The maximum distance among the centroids for the trapezium was 3.5 mm. On the metacarpal bone, the maximum distance was 6.7 mm, which was almost twice that of the trapezium.

cycle) flexion-extension motion through a maximum arc of 30° (10° of flexion and 20° of extension). Accuracies were evaluated against a benchmark based on the positions of the centroids of bone-fixed beads. Four Teflon beads (spheres, 3 mm in diameter), which are radiopaque on CT, were rigidly fixed to the first metacarpal and trapezium. The cadaver was scanned using the same 4-D CT procedure used in the in vivo study. Transformations of the centroids of the markers were obtained using the registration technique to express the error relative to the benchmark.

Table 1. Thumb kinematics obtained using an Euler angle ZX′Y″ sequence and the magnitude of translations of the center of the articular surfaces

Thumb movement	Rotation (degrees)			Translation of center of estimated joint contact area (mm)
	Flexion/extension	Pronation/supination	Abduction/adduction	
Initial key pinch position → adduction	−22.5	1.8	29.0	4.1
Adduction → palmar abduction	11.6	3.3	−37.9	4.0
Palmar abduction → opposition	9.3	11.5	−16.7	1.0
Opposition → initial key pinch position	−4.8	1.5	25.3	1.5

Results

During thumb circumduction, the first metacarpal bone of the thumb articulated with the trapezium, extending 22.5° from the initial key pinch position in the adduction direction. It then flexed 11.6°, flexed 9.3°, and finally extended 4.8° during each increment of the movement (Table 1). Regarding pronation-supination, the range of metacarpal bone pronation was 1.5° to 11.5°. The rotation in palmar abduction-adduction was the largest of the three rotation components (−37.9° to 29°). The magnitude of the translation of the center of the estimated joint contact area of the metacarpal was 4.1, 4.0, 1.0, and 1.5 mm when moving from the initial key pinch position to the adduction, then, adduction to palmar abduction, and then palmar abduction to opposition, and opposition to the initial key pinch position, respectively.

The estimated joint contact areas of the trapezium and metacarpal bones for each thumb position were displayed using a color scale ranging from 0 mm to 3 mm (Fig. 2). Except for adduction, central-volar contact patterns were observed on both the trapezium and the metacarpal bones. Also, the estimated joint contact area in the position of opposition was along the radiovolar perimeter of the thumb CMC joint. In the initial key pinch position, the average of the estimated joint contact areas on the trapezium was 69 mm^2 (± 8.3) (within a 1-mm threshold) (Fig. 3). The position of adduction had the smallest contact area of any position (57 mm^2) and was located on the dorsal-central portion of the trapezium articular surface. The maximum contact area occurred in the palmar abduction position (76 mm^2) on the radiocentral portion of the articular surface. The average of the estimated joint contact areas on the metacarpal bone was 68 mm^2 (± 9.9). The minimum contact area on the metacarpal bone was 55 mm^2 and was located in the midportion of the radial side of the bone in the adduction thumb position. The maximum contact area was 77 mm^2 and was located in the center of the metacarpal articular surface in the palmar abduction position.

For the distribution ratios of the estimated joint contact areas, central-volar contact patterns were observed on both the trapezium and the metacarpal bone except for in adduction. The estimated contact area centroids for each thumb position were determined from each estimated joint contact area within a 1-mm threshold (Fig. 4). The centroids on the trapezium were located in the central zone of the articular surface. The centroid on the trapezium was characterized by movement in a volar and dorsal direction during the thumb circumduction motion. Meanwhile, the centroid on the metacarpal bone moved in a radial and ulnar direction. The maximum distance traversed by the centroids on the trapezium was 3.5 mm. With respect to the metacarpal bone, the maximum distance was 6.7 mm, which was almost twice the magnitude of that of the trapezium.

The in vitro cadaveric validation of CMC motion for this voxel-based registration technique using fiducial markers revealed an average rotational error of 0.59° (± 0.5) and an average translation error of 0.66 mm (± 0.62) for the metacarpal and 0.36° (± 0.37) and 0.28 mm (± 0.3) for the trapezium.

Discussion

The articular surfaces of the CMC joint have been described as saddle-shaped, ie, they show a convex curve on one axis and a concave curve about the other [13]. The mobility of the thumb CMC joint is derived from the differing radii of curvature of its saddle shape, whereas the stability of this joint is largely dependent on soft ligamentous-capsule support and muscle tendon action. The joint stability provided from soft tissues is achieved by a complex balance between static (capsule and ligaments) and dynamic muscle-tendon soft tissue stabilizers. This relative stabilizing effect varies according to the joint position, motion, and load to the joint. Therefore, pathological conditions that cause interruption of the soft tissues and subsequently dynamic instability are difficult to diagnose using conventional examination protocols such as routine radiographs or CT. The instability of the thumb CMC joint resulting from incompetent or slack ligaments

has been suggested to be responsible for initiation and progression to degenerative osteoarthritis [6, 9]. Joint instability, therefore, might best be evaluated using in vivo dynamic measurements. We developed this in vivo dynamic measurement to quantify thumb circumduction, which enabled us to display and analyze the results obtained from the measurements three-dimensionally.

This study had a number of limitations. First, a limiting factor of the 4-D CT imaging is its temporal resolution, resulting in some motion artifacts, which depended on the motion velocity of the bones. However, if subjects move smoothly and at a constant speed, the image artifact at the CMC joint should be minimal given the small ROM at the joint. Furthermore, we anticipate that advances in CT technology such as faster temporal resolution will further improve dynamic CMC imaging. Second, the measurement of the estimated joint contact area is inherently limited because it does not take into consideration the thickness of the cartilage. However, because the cartilage thickness is not known to vary considerably across the joint surface, the study findings are credible. Furthermore, we cannot yet make definitive statements about the arthrokinematics of the CMC joint because our data are preliminary and limited to a single healthy subject; this study can be seen as a kind of proof of concept, demonstrating both technical feasibility and accuracy as compared with a dynamic cadaver model. Additional subjects will be required to build a normative database.

Other methods exist to capture dynamic movements of the CMC joint; however, they are unable to capture the true arthrokinematics at the joint. Surface-based motion capture is prone to skin motion artifact, which is considerable given the depth of the trapezium and proximal first metacarpal. Even if this artifact could be mitigated, some form of medical imaging would still be necessary to image the articular surfaces. Dynamic xray and fluoroscopy are useful modalities for evaluating osseous motion in larger joints; however, their planar nature makes segmentation and registration difficult in regions of bony overlap such as the wrist. MRI can be used for some dynamic imaging; however, it has limitations. In general, MRI dynamic imaging (cine MRI) is usually limited to two-dimensional images with thicker slices. Therefore, it does not provide 3-D images with sufficient isotropic resolution along all three dimensions. Multiprojection image intensifiers also provide 4-D imaging [4]. However, it has poorer spatial resolution owing to the low number of projections used to reconstruct a 3-D image. Finally, although quasistatic motion analysis from a series of static 3-D images has high spatial resolution, dynamic kinematic and kinetic factors such as muscle loading are not realistically incorporated.

Circumduction motion at the CMC joint distinguishes the thumb from the other four fingers and is an important function for daily activities. Circumduction is a composite action that involves two main axes of movement: flexion-extension and adduction-abduction (with a small amount of axial rotation). To achieve this complex motion, the CMC of the thumb has a unique geometrical (saddle) shape. Unfortunately, the same geometry that facilitates this motion [13] results in reduced contact areas between the articulating surfaces, resulting in joint compressive loads being transferred through reduced contact areas. Consequently, high contact stresses occur at the thumb CMC joint, which may lead to degenerative joint disease. In addition, the shear stresses in this area are increased by laxity of the volar-anterior or palmar beak ligaments [14].

The median arcs of the thumb CMC joint have been reported to be 53° of flexion-extension, 42° of abduction-adduction, and 17° of pronation-supination [5]. Our arthrokinematics were in general agreement; however, because the study focused on one subject, individual differences may explain the difference. The estimated joint contact areas were concentrated on the central-volar region of the trapezium except when the thumb was in excessive adduction. Degenerative osteoarthritis has been reported to occur in this region [14]. We believe, therefore, that our results appear consistent with a characteristic pattern of osteoarthritic lesions. As for the movement of the contact area centroids, on the trapezium, the centroid exhibited movement in a volar and dorsal direction during the thumb circumduction. Meanwhile, the centroid on the metacarpal bone moved in a radial and ulnar direction. We think that this movement pattern indicates the incongruous nature of the articular surface and saddle joint geometry in which the motion is affected by the opposition of two surfaces, each of which is concave in one direction and convex in the other.

To our knowledge, there are no in vivo data estimating joint contact areas and distribution ratios during thumb circumduction. Quantification of estimated joint contact areas throughout joint motion provides insight into the role of CMC joint biomechanics; future studies may be able to use this technique to identify some of the factors that predispose patients to osteoarthritis. This analysis approach provides a tool to assess the estimated joint contact characteristics in vivo under actual muscle-loading conditions. Further analysis using dynamic CT imaging may serve to further clarify basilar thumb joint kinetics and help us to devise improved anatomic surgical reconstructions.

References

1. Adams R, Bischof L. Seeded region growing. *IEEE Transactions on Pattern Analysis and Machine Intelligence.* 1994;16:641–647.
2. Ateshian GA, Ark JW, Rosenwasser MP, Pawluk RJ, Soslowsky LJ, Mow VC. Contact areas in the thumb carpometacarpal joint. *J Orthop Res.* 1995;13:450–458.

3. Biswas D, Bible JE, Bohan M, Simpson AK, Whang PG, Grauer JN. Radiation exposure from musculoskeletal computerized tomographic scans. *J Bone Joint Surg Am.* 2009;91:1882–1889.
4. Carelsen B, Bakker NH, Strackee SD, Boon SN, Maas M, Sabczynski J, Grimbergen CA, Streekstra GJ. 4D rotational x-ray imaging of wrist joint dynamic motion. *Med Phys.* 2005;32: 2771–2776.
5. Cooney WP 3rd, Lucca MJ, Chao EY, Linscheid RL. The kinesiology of the thumb trapeziometacarpal joint. *J Bone Joint Surg Am.* 1981;63:1371–1381.
6. Eaton RG, Littler JW. Ligament reconstruction for the painful thumb carpometacarpal joint. *J Bone Joint Surg Am.* 1973;55: 1655–1666.
7. Hajnal JV, Saeed N, Soar EJ, Oatridge A, Young IR, Bydder GM. A registration and interpolation procedure for subvoxel matching of serially acquired MR images. *J Comput Assist Tomogr.* 1995; 19:289–296.
8. Hill DL, Batchelor PG, Holden M, Hawkes DJ. Medical image registration. *Phys Med Biol.* 2001;46:R1–45.
9. Jonsson H, Valtysdottir ST, Kjartansson O, Brekkan A. Hypermobility associated with osteoarthritis of the thumb base: a clinical and radiological subset of hand osteoarthritis. *Ann Rheum Dis.* 1996;55:540–543.
10. Leng S, Zhao K, Qu M, An KN, Berger R, McCollough CH. Dynamic CT technique for assessment of wrist joint instabilities. *Med Phys.* 2011;38(Suppl 1):S50.
11. Lorensen WE, Cline HE. Marching cubes: a high resolution 3D surface construction algorithm. *Comput Graph.* 1987;21:163–170.
12. Mehnert A, Jackway P. An improved seeded region growing. *Pattern Recognition Letters.* 1997;18:1065–1071.
13. Napier JR. The form and function of the carpo-metacarpal joint of the thumb. *J Anat.* 1955;89:362–369.
14. Pellegrini VD Jr. Osteoarthritis of the trapeziometacarpal joint: the pathophysiology of articular cartilage degeneration. I. Anatomy and pathology of the aging joint. *J Hand Surg Am.* 1991; 16:967–974.
15. Wu G, van der Helm FC, Veeger HE, Makhsous M, Van Roy P, Anglin C, Nagels J, Karduna AR, McQuade K, Wang X, Werner FW, Buchholz B. ISB recommendation on definitions of joint coordinate systems of various joints for the reporting of human joint motion—Part II: shoulder, elbow, wrist and hand. *J Biomech.* 2005;38:981–992.